Parameter De-Embedding Accuracy Dependency Upon Material Sample Dimensions

A. Park and Allen Dominek

Abstract—**The sensitivity of the sample fit in rectangular waveguide fixtures is examined for constitutive parameter de-embedding. The sensitivity is characterized through a percent error figure between the de-embedded and known parameter values when an air gap exists between the sample and the side walls of the fixture. The de-embedding process assumed a completely filled waveguide in which rigorously calculated *S* parameters for material sample air gaps in either the E or H plane walls of the waveguide were used. The presence of an air gap was very noticeable for a E-plane gap. Commonly used gap correction factors provided limited improvement in reducing air gap related errors.**

I. Introduction

A VARIETY of techniques are available for de-embedding the constitutive parameters from a material sample [1]. One of the most useful approaches involves the transmission line concepts for single mode operation. This approach has become convenient with the advent of automatic network analyzers for broadband results [2]. Two common fixtures for this approach utilize coaxial or rectangular cross sections. A concern for these fixtures is that the sample should have a good cross sectional fit to avoid any air gaps between the sample and fixture. The limitation of having a poorly fitting sample arises in that the measured responses are not necessarily the anticipated responses.

The presence of air gaps may even be desirable for very high temperature measurements due to sample expansion. Preparing a sample to properly fit at ambient temperatures most likely results in a very tight fitting sample at elevated temperatures. This often results in unremovable samples after the measurement without destroying them. Allowing an appropriate air gap at ambient temperatures can relax this inconvenience. However, the need to correct for de-embedded constitutive parameters in the presence of sample air gaps exists for temperatures between the ambient temperature and the highest temperature of interest.

A study is presented to demonstrate the effect of the presence of canonical air gaps between the sample and fixture walls. The air gaps examined are shown in Fig. 1

Manuscript received April 2, 1991; revised January 21, 1992.

The authors are with the ElectroScience Laboratory, Department of Electrical Engineering, The Ohio State University, Columbus, OH 43212.

IEEE Log Number 9200855.

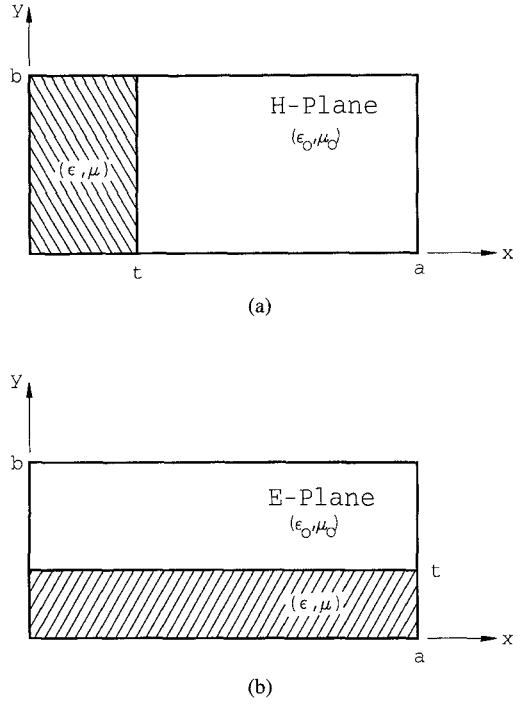

Fig. 1. Illustration of evaluated cross sectional air gaps. (a) H-plane. (b) E-plane.

for material samples with complex constitutive parameters. Air gaps for actual material samples are not as simple as these canonical air gaps but their effect can be characterized by these canonical air gaps. This study yields parameter errors for de-embedded parameters using calculated reflection and transmission responses with known air gaps. The de-embedding expressions used to obtain the parameters were based upon a completely filled cross section to demonstrate the significance of air gaps. The calculated reflection and transmission responses were generated from moment method (modal matching) solutions.

Additional comparisons are also made to determine the effectiveness of known expressions to correct the error associated with an air gap [3], [4]. Other works [5]–[7] have also considered the use of these correction factors. Only [5] demonstrates the accuracy of three expressions for E-plane gaps based upon measurements. In this work, both H and E plane gaps for rectangular waveguide samples are considered.

0018-9480/92$03.00 © 1992 IEEE

II. Procedure

A general moment method solution for the reflected and transmitted fields of a partially filled, finite length rectangular waveguide section was created. This solution provided convenient numerical results for the necessary fields involving air gaps of any size. These results were then used in the explicit expressions for the de-embedding of material parameters when the cross section is completely filled. These de-embedded parameters were normalized to the values initially used to generate a percent error value. The percent error values are defined as

$$\% \text{ Error} = \frac{X_{\text{ext}} - X_{\text{exa}}}{X_{\text{exa}}} \tag{1}$$

where X_{ext} and X_{exa} represent either the real or imaginary components of the de-embedded and exact parameters, respectively.

The notation for the relative constitutive parameters are the traditional symbols of ϵ_r for permittivity and μ_r for permeability. As shown in Fig. 1, the cross sectional dimensions of the waveguide are given by a and b with the material thickness given by t. The sample length is denoted by d.

A. De-Embedding Expressions

The common expressions used to de-embed the relative constitutive parameters from waveguide reflection (S_{11}) and transmission (S_{21}) measurements are given below:

$$\mu_r = \frac{1 + \Gamma}{1 - \Gamma} \frac{\lambda_o}{\Lambda X_o} \tag{2}$$

and

$$\epsilon_r = \left(\frac{1}{\Lambda^2} + \frac{1}{(2a)^2} \right) \frac{\lambda_o^2}{\mu_r} \tag{3}$$

where

$$\Gamma = K \pm \sqrt{K^2 - 1} \tag{4}$$

with

$$K = \frac{S_{11}^2 - S_{21}^2 + 1}{2S_{11}}, \tag{5}$$

$$\frac{1}{\Lambda^2} = -\left[\frac{1}{2\pi d} \ln \frac{1}{P} \right]^2 \tag{6}$$

and

$$P = \frac{S_{11} + S_{21} - \Gamma}{1 - (S_{11} + S_{21})\Gamma}. \tag{7}$$

where λ_o is the free space wavelength for the desired measurement frequency. The quantities, Γ and P, correspond to the reflection coefficient from a semi-infinite material interface and the propagation factor for a wave in the material. Note that the sign in (4) is chosen to insure $|\Gamma| \leq 1$, and that $\ln(1/P)$ is modulo $j2\pi n$ where n is the integer of (d/λ_g) (λ_g is the guide wavelength in the filled portion of the guide). The proper value of n can be estimated with the integer value of

$$n = \text{Int} \left[\frac{f\Phi'}{2\pi} \right] \tag{8}$$

where Φ' is the derivative (slope) of the phase for the propagation factor P with respect to frequency and f is frequency.

These expressions are limited to the existence of only one mode in either the unfilled or filled portions of the sample fixture. Under ideal conditions, no higher order modes can be excited in the filled portion even when their cutoff frequency is below the measurement frequency.

B. S-Parameters

The S parameter expressions for a material sample in a completely filled rectangular waveguide with only one propagating mode in each region are very simple and are given below:

$$S_{11} = \frac{(1 - P^2(\epsilon_r, \mu_r))\, \Gamma(\epsilon_r, \mu_r)}{(1 - P^2(\epsilon_r, \mu_r)\, \Gamma^2(\epsilon_r, \mu_r))} \tag{9}$$

and

$$S_{21} = \frac{(1 - \Gamma^2(\epsilon_r, \mu_r))\, P(\epsilon_r, \mu_r)}{(1 - P^2(\epsilon_r, \mu_r)\, \Gamma^2(\epsilon_r, \mu_r))} \tag{10}$$

with

$$P = \exp\left(-j \frac{2\pi}{\lambda_o} X_1 \sqrt{\epsilon_r \mu_r}\, d \right) \tag{11}$$

and

$$\Gamma = \frac{\sqrt{\frac{\mu_r}{\epsilon_r} \frac{X_o}{X_1}} - 1}{\sqrt{\frac{\mu_r}{\epsilon_r} \frac{X_o}{X_1}} + 1} \tag{12}$$

where $X_o = \sqrt{1 - (\lambda_o/2a)^2}$ and $X_1 = \sqrt{1 - [(\lambda_o/2a\sqrt{\epsilon_r \mu_r})]^2}$.

The presence of an air gap as shown in Fig. 1 may allow several propagating modes to exist in the filled portion of the waveguide and equally as important, evanescent modes have to be considered to satisfy the boundary conditions at the sample interfaces along the length of the guide. The field solutions for these two geometries were generated using a two step process. First, a modal matching was performed for a single semi-infinite air-material interface as shown in Fig. 2 to generate the complete scattering matrix, s_{ij}. The fields in each region were expanded using entire basis functions as was done in [8], [9] for the different cross sectional geometries. The required propagation constants for the filled regions were numerically found through solving the pertinent transcendental equations [10], [11].

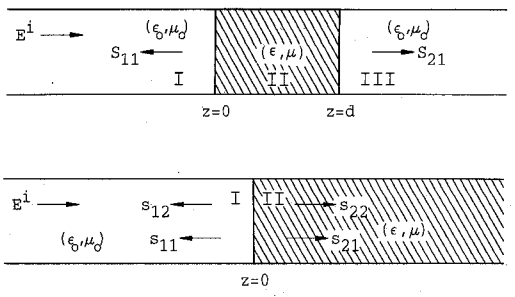

Fig. 2. Waveguide regions.

The second step utilized a self-consistent formulation [12] with the scattering parameters for the semi-infinite case to provide the reflection and transmission responses of a finite length sample by considering all the interactions between the two sample faces. The appropriate self-consistent expressions are

$$S_{11} = [s_{11}] + [s_{12}][P][s_{22}][P] \cdot (I - [s_{22}][P][s_{22}][P])^{-1}[s_{21}] \quad (13)$$

and

$$S_{21} = [s_{12}][P](I - [s_{22}][P][s_{22}][P])^{-1}[s_{21}]. \quad (14)$$

The diagonal matrix, $[P]$, is the modal propagation matrix where each element corresponds to the propagation factor for each mode. The details for the complete solution are provided in [13]. The solution has been confirmed through several measurements involving partially filled rectangular waveguides.

C. Air Gap Correction Expressions

The presence of a narrow air gap can allow first order correction factors to be used in an attempt to improve upon the accuracy of de-embedded parameters. Correction expressions in [3], [4] for an E-plane air gap are based upon the effective capaitance of two series capacitors. In this approach, the measured ϵ_r is related to the effective capacitance for a parallel plate capacitor with plate separation distance of b. A corrected ϵ_r value can be obtained by solving for the ϵ_r value of the modeled capacitor filled with the material of unknown parameter value. The form of the given expressions in [3], [4] is quite complicated since they are presented in rectangular form. The Appendix demonstrates the derivation for the ϵ case.

The correction factors of the parameters for both E- and H-plane geometries are given below:

H-Plane

$$\epsilon_r^c = \frac{2\epsilon_r^m - \left(1 + \cos\frac{\pi}{a}t\right)}{1 - \cos\frac{\pi}{a}t} \quad (15)$$

$$\mu_r^c = \frac{\mu_r^m t}{a - \mu_r^m(a - t)} \quad (16)$$

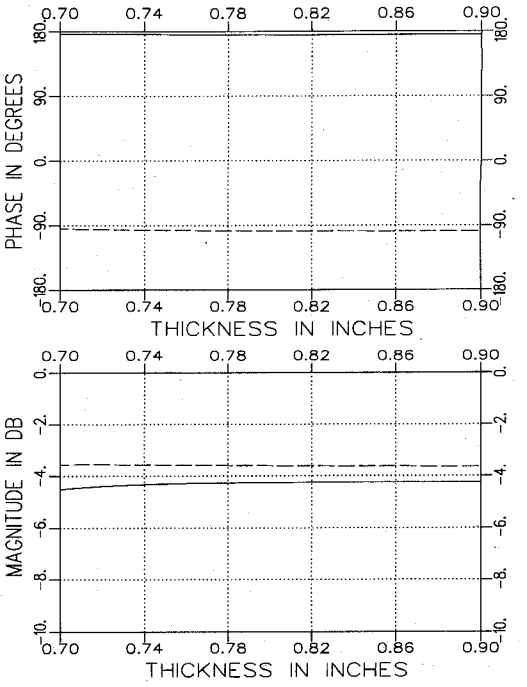

Fig. 3. Calculated S_{11} (solid) and S_{21} (dashed) for varying t with $\epsilon_r = (4.0, -j.20)$, $\mu_r = (1.2, -j.12)$, $d = .156''$ and $f = 10$ GHz. H-plane geometry.

E-Plane

$$\epsilon_r^c = \frac{\epsilon_r^m t}{b - \epsilon_r^m(b - t)t} \quad (17)$$

$$\mu_r^c = \frac{2\mu_r^m - \left(1 + \cos\frac{\pi}{a}t\right)}{1 - \cos\frac{\pi}{a}t} \quad (18)$$

where the superscripts m and c refer to measured and corrected values, respectively. These expressions were derived by considering effective capacitors and magnetic resistors in series or parallel connections.

III. Results

The first set of figures demonstrate the reflection and transmission responses as a function of material thickness, t. Figs. 3 and 4 demonstrate the effect for H and E-plane material samples, respectively, at 10 GHz for a X-band waveguide ($.4'' \times .9''$). The sample is $d = .156''$ long with $\epsilon_r = (4.0, -j.20)$, $\mu_r = (1.2, -j.12)$. Note that the H-plane sample is rather insensitive to any air gap while the E-plane is very sensitive for any small gaps as expected. This behavior is invariant even for magnetically dominated material.

The next set of figures are normalized percent errors for the direct de-embedded corrected constitutive parameters for the responses shown in Figs. 3 and 4. The direct parameter values were obtained from (2) and (3) and the corrected parameter values were obtained from (15) through (18). Figs. 5 and 6 pertain to ϵ_r and μ_r values, respectively, for an H-plane air gap. Figs. 7 and 8 pertain

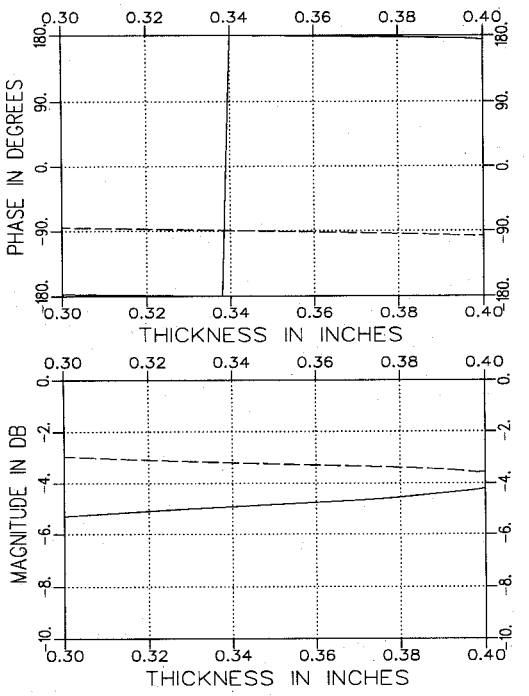

Fig. 4. Calculated S_{11} (solid) and S_{21} (dashed) for varying t with $\epsilon_r = (4.0, -j.20)$, $\mu_r = (1.2, -j.12)$, $d = .156''$ and $f = 10$ GHz. E-plane geometry.

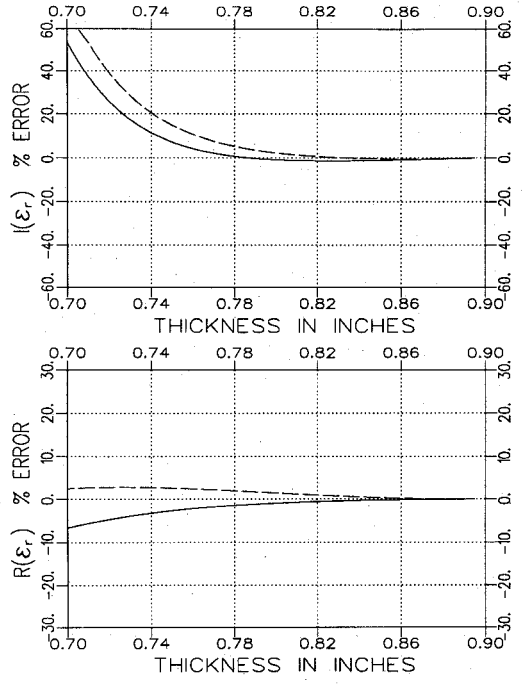

Fig. 5. Normalized percent error in ϵ_r for a partially filled waveguide of thickness t at 10 GHz with $\epsilon_r = (4.0, -j.20)$, $\mu_r = (1.2, -j.12)$ and $d = .156''$. H-plane geometry. Solid-direct, dashed-corrected values.

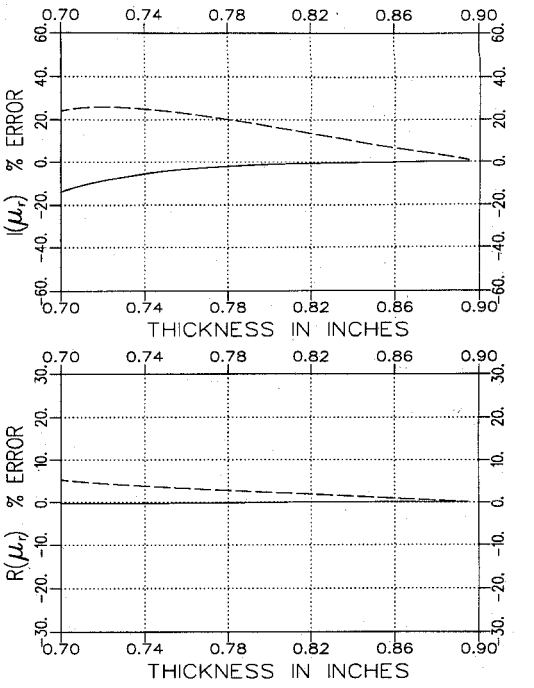

Fig. 6. Normalized percent error in μ_r for a partially filled waveguide of thickness t at 10 GHz with $\epsilon_r = (4.0, -j.20)$, $\mu_r = (1.2, -j.12)$ and $d = .156''$. H-plane geometry. Solid-direct, dashed-corrected values.

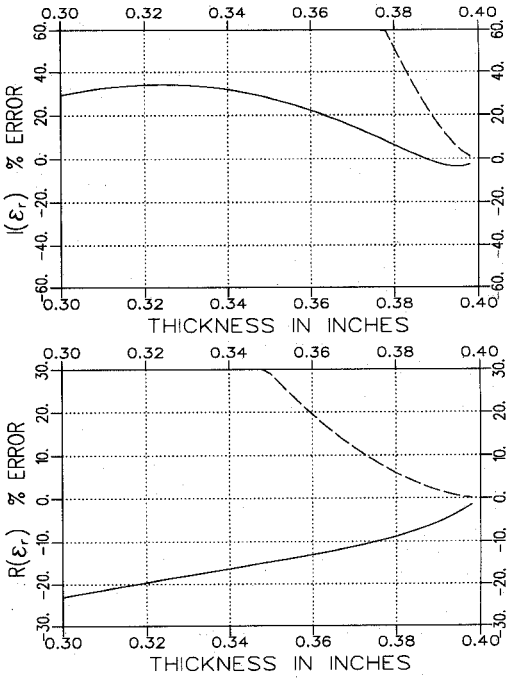

Fig. 7. Normalized percent error in ϵ_r for a partially filled waveguide of thickness t at 10 GHz with $\epsilon_r = (4.0, -j.20)$, $\mu_r = (1.2, -j.12)$ and $d = .156''$. E-plane geometry. Solid-direct, dashed-corrected values.

to ϵ_r and μ_r values, respectively, for an E-plane air gap. As stated earlier, the reflection and transmission responses were generated using (13) and (14) and the moment method results for the actual air gap geometries. These figures demonstrate the influence of an air gap on the de-embedded parameters and the limitations of the correction factors. The H-plane correction factors actually degraded the accuracy of de-embedded parameters while the E-plane correction factors did improve the parameter accuracy for very thin air gaps. As can be expected, the usefulness of the correction factors readily degrade when the constitutive parameter values increase from the values used here.

The final set of figures are normalized percent errors for the direct de-embedded and corrected constitutive parameters for responses with a material sample air gap of

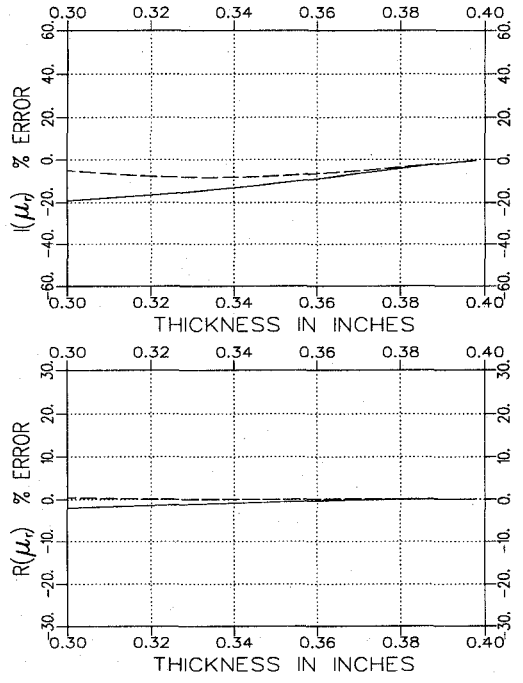

Fig. 8. Normalized percent error in μ_r for a partially filled waveguide of thickness t at 10 GHz with $\epsilon_r = (4.0, -j.20)$, $\mu_r = (1.2, -j.12)$ and $d = .156''$. E-plane geometry. Solid-direct, dashed-corrected values.

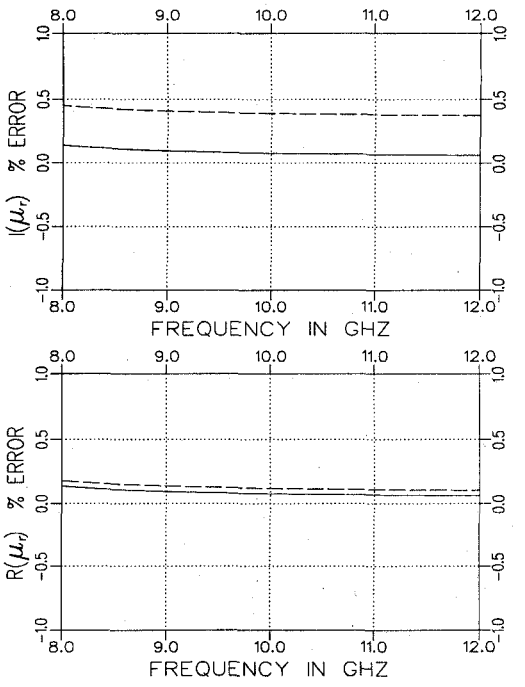

Fig. 10. Normalized percent error in μ_r for an .002″ air gap along the short wall for a rectangular guide with $\epsilon_r = (4.0, -j.20)$, $\mu_r = (1.2, -j.12)$ and $d = .156''$. H-plane geometry. Solid-direct, dashed-corrected values.

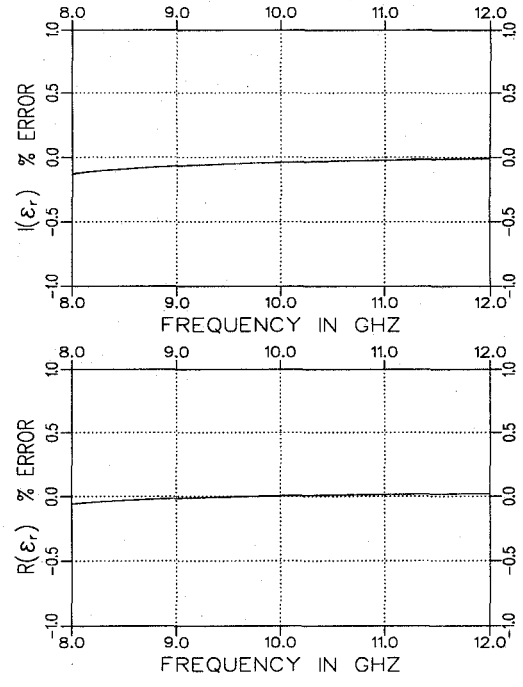

Fig. 9. Normalized percent error in ϵ_r for an .002″ air gap along the short wall for a rectangular guide with $\epsilon_r = (4.0, -j.20)$, $\mu_r = (1.2, -j.12)$ and $d = .156''$. H-plane geometry. Solid-direct, dashed-corrected values (both overlap).

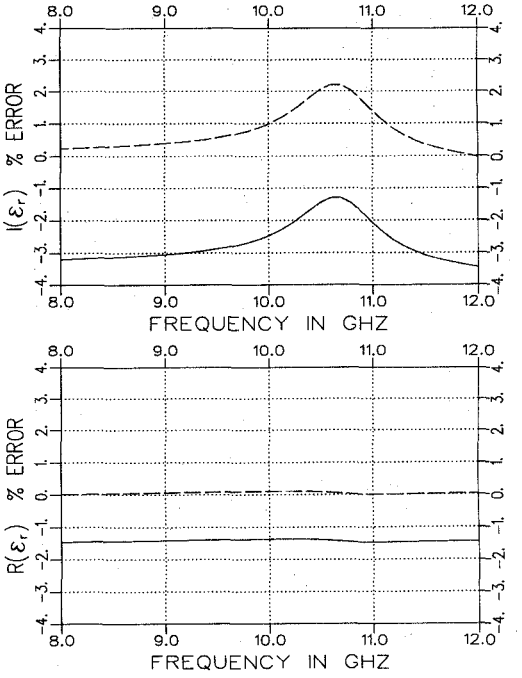

Fig. 11. Normalized percent error in ϵ_r for an .002″ air gap along the long wall for a rectangular guide with $\epsilon_r = (4.0, -j.20)$, $\mu_r = (1.2, -j.12)$ and $d = .156''$. E-plane geometry. Solid-direct, dashed-corrected values.

.002″ between 8 and 12 GHz. Figs. 9 and 10 illustrate the percent error for ϵ_r and μ_r with an H-plane geometry, respectively. Figs. 11 and 12 illustrate the percent error for ϵ_r and μ_r with an E-plane geometry. The relative contitutive parameters were again $\epsilon_r = (4.0, -j.20)$, $\mu_r = (1.2, -j.12)$ with $d = .156''$. As expected, the E-plane sample geometry experienced more error. The ability for the correction factors to be useful as a function of frequency is limited as shown in these figures since they were based upon static approximations.

Naturally, these results for this one material parameter set does not completely characterize the potential error that can be experienced due to an improper fitted sample. However, it does represent the typical errors due to air

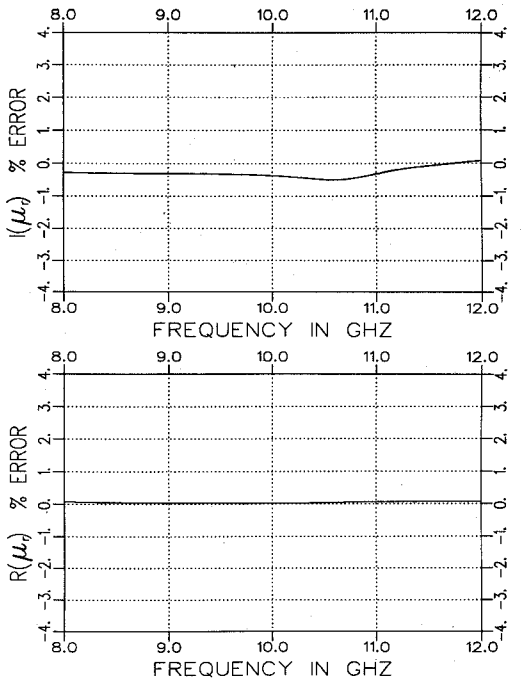

Fig. 12. Normalized percent error in μ_r for an .002″ air gap along the long wall for a rectangular guide with $\epsilon_r = (4.0, -j.20)$, $\mu_r = (1.2, -j.12)$ and $d = .156''$. E-plane geometry. Solid-direct, dashed-corrected values (both overlap).

gaps and this error is of the same order as other errors (such as hardware and calibration accuracies) which can occur in broadband measurements.

IV. Conclusions

A small H-plane air gap in a material sample is essentially insignificant. The same can not be said for an E-plane air gap where the electric field of the dominant mode is normal to an air gap interface. The same results also occur when the material has μ_r values significantly different from unity. Extending these results to a material sample for a coaxial fixture indicates that significant error can also be experienced. This extrapolation is based upon the orientation of the electric field with respect to any potential air gap interface.

The correction of de-embedded parameters due to the influence of air gaps using static models is of limited value. This approach appeared to have no real overall improvement capability in achieving a better estimate for the de-embedded parameter values. Actually, greater error usually resulted. Attempting greater accuracy through using a one mode expansion for the solution of the reflected and transmitted fields in place of the expressions given in (9) through (12) for the two canonical geometries does not help. The H-plane one mode approximation reduces to the completely filled result while the E-plane approximation requires at least three modes for satisfactory results based upon the numerical values of the modal propagation constants in the partially filled regions. The de-embedding of constitutve parameters in the presence of known air gaps appears to be confined through an iterative search using measured and calculated reflection and transmission responses for a given geometry [13].

Appendix

The static correction approximation for estimating the ϵ constitutive parameter values for both generic partially filled geometries is derived here. A similar procedure is used to determine the correction approximation for μ using magnetic circuit resistances. The simplest derivation is for the E plane approximation where two series capacitors are assumed. The circuit expression for this case is

$$\frac{1}{C_m} = \frac{1}{C_d} + \frac{1}{C_o} \tag{19}$$

where $C = (\epsilon A/h)$ is the capacitance for each region with A being the surface area of the effective capacitor and h being the material thickness. The subscripts d and o refer to the actual dielectric values for the filled and air gap regions, respectively and m refers to the assumed capacitance from the de-embedding procedure. Reducing the above expression yields the expression given in (17).

The H-plane expression is slightly more involved since the field distribution is not the same across both faces of the effective capacitors. In this case, there are two capacitors in parallel as expressed below.

$$C_m = C_d + C_o. \tag{20}$$

The desired expression shown in (15) for the H-plane result was obtained by calculating the charge, Q, and plate voltage, V, for each effective capacitor, $C = (Q/V)$ assuming an electric field distribution of $E_x = E_o \sin(\pi/a)x$. The charge for the total configuration was calculated by

$$Q = \epsilon\, d \int_0^t E_x\, dx + \epsilon_o\, d \int_t^a E_x\, dx \tag{21}$$

which yields

$$Q = -\epsilon\, d \frac{a}{\pi} E_o \left[\cos\frac{\pi}{a} t - 1\right] - \epsilon_o\, d \frac{a}{\pi} E_o \left[-1 - \cos\frac{\pi}{a} t\right]. \tag{22}$$

The charge expressions for the individual regions follow the same procedure. The effective average voltage for all three capacitors is simply

$$\hat{V} = \frac{1}{a} \int_x \int_y E_x\, dx\, dy \tag{23}$$

which reduces to $\hat{V} = (2/\pi) b E_o$. Inserting these expressions into (20) results in (15).

References

[1] M. N. Afsar, J. R. Birch and R. N. Clarke, "The measurement of the properties of material," *Proc. IEEE*, vol. 74, no. 1, pp. 183–199, Jan. 1986.

[2] *HP Product Note 8510-3*, "Measuring dielectric constant with the HP 8510 network analyzer," Hewlett-Packard Company.

[3] W. B. Westphal, "Techniques of measuring the permittivity and permeability of liquids and solids in the frequency range 3 C/S to 50 KMC/S," Report No. 36, July 1950, Laboratory for Insulation Research, Massachusetts Institute of Technology; Prepared under O.N.R. contract N5ori-07801.

[4] *Handbook of Microwave Measurements*, M. Wind and H. Rapaport, Ed., Polytechnic Institute of Brooklyn, vol. 1, section X, appendix I, p. 29, 1955.

[5] K. S. Champlin and B. H. Glover, "Gap effects' in measurement of large permittivities," *IEEE Trans. Microwave Theory Tech.*, vol. MTT-14, pp. 397–398, Aug. 1966.

[6] S. B. Wilson, "Modal analysis of the 'gap effect' in waveguide dielectric measurements," *IEEE Trans. Microwave Theory Tech.*, vol. 36, pp. 752–756, Apr. 1988.

[7] K. E. Mattar, D. G. Watters, and M. E. Brodwin, "Influence of wall contacts on measured complex permittivity spectra at coaxial line frequencies," *IEEE Trans. Microwave Theory Tech.*, vol. 39, pp. 532–537, Mar. 1991.

[8] R. E. Collin, *Theory of Guided Waves*. New York: McGraw-Hill, 1960, Ch. 6 and 8.

[9] R. E. Collin and R. M. Vaillancourt, "Application of Rayleigh-Ritz method to dielectric steps in waveguides," *IRE Trans. Microwave Theory Tech.*, vol. MTT-5, pp. 177–184, July 1957.

[10] R. F. Harrington, *Time-Harmonic Electromagnetic Fields*. New York: McGraw-Hill, pp. 158–163, 1961.

[11] M. Razaz and J. B. Davies, "Analysis of rectangular waveguide partially loaded with lossy dielectric," *Proc. Inst. Elec. Eng.*, M.O.A., vol. 2, no. 1, pp. 1–5, Jan. 1978.

[12] A. Altintas, P. H. Pathak, and W. D. Burnside, "Electromagnetic scattering from a class of open-ended waveguide discontinuities," Rep. 716148-9, ElectroScience Laboratory, The Ohio State University, pp. 16–26, Mar. 1986.

[13] A. Park and A. Dominek, "Constitutive parameter de-embedding using inhomogeneously filled rectangular waveguides with longitudinal sectional modes," Rep. 721837-2, ElectroScience Laboratory, Department of Electrical Engineering, The Ohio State University, Oct. 1990; Prepared under NASA Lewis Research Grant NAG3-1000.

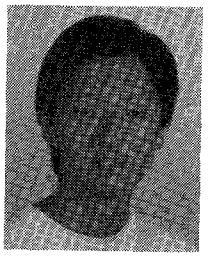

Albert Park received the B.S. degree in Engineering Physics from the Miami University in 1986 and the M.S.E.E. degree from The Ohio State University in 1990.

From 1986 to 1990, he was at the ElectroScience Laboratory of The Ohio State University as a Graduate Research Associate. His activities involve him in experimental and numerical material analysis for scattering applications.

Allen Dominek received the B.S.E.E. and M.S.E.E. degrees from the University of North Dakota in 1978 and 1980, respectively, and the Ph.D. degree from The Ohio State University in 1984.

From 1980 to 1984, he was at the ElectroScience Laboratory of the Ohio State University as a Graduate Research Associate. He is currently a Senior Research Associate at the ElectroScience Laboratory, with interests in numerical and experimental techniques involving scattering and radiation.